Scattering from PEC Cylinders by a Normally Incident Plane Wave

Paul Tsuji, Kristen Parrish, and Chicheng Xu

***Abstract*—The method of moments (MOM) is implemented to simulate scattering from two types of PEC objects: circular cylinders and square cylinders. In order to gauge the accuracy of the MOM algorithms used, an exact analytical solution is used for the cylinder problem, and reference papers are used for the square cylinders. The computational complexity of these methods is also examined, with both a direct solver and an iterative solver.**

I. Introduction

The Method of Moments (MOM) is a boundary element method, a numerical method of solving linear partial differential equations in boundary integral form. It is often applied to integral equations, where the kernel is a Green's function, to solve scattering problems involving complex objects [1, 2].

In this paper, the MOM is implemented to simulate scattering from an obliquely incident plane wave onto 2-D PEC cylinders. To gauge the performance of the MOM algorithm with a circular cylinder geometry, results are compared to an exact analytical solution. For the square cylinder, published works are used to gauge the accuracy of the results. The computational complexity and possible improvements for each method are discussed and the strengths and weaknesses of the various methods are discussed.

II. Formulation

A. Problem Statement

A plane wave is incident on a PEC cylinder invariant in the z direction. Both circular cylinders of radius a and square cylinders of side length $2a$ are simulated, as shown in Figures 1 and 2. The electric current density induced on the surface of each cylinder is calculated, as is the bistatic echo width (radar cross section or RCS) with respect to angle ϕ. The analytical solutions for scattering from circular cylinders for both TE_z and TM_z polarizations are presented in the following section. An analytical solution for scattering from a square cylinder is not available; however, results from other works are presented in later sections for comparison. The geometries of the cylinders are defined such the incident wave hits the cylinder at $\phi = 180\,^\circ$, as indicated in Figures 1 and 2.

B. Analytical Solution for Circular PEC Cylinders

The TE_z case is derived first, in cylindrical coordinates. The incident magnetic field can be written as an infinite sum of Bessel functions [3],

$$\overrightarrow{H}^i = \widehat{a}_z H_0 e^{-j\beta\rho\cos\phi} \quad (1)$$

$$= \widehat{a}_z H_0 \sum_{n=0}^{n=\infty} (-j)^{-n} \varepsilon_n J_n(\beta\rho)\cos(n\phi) \quad (2)$$

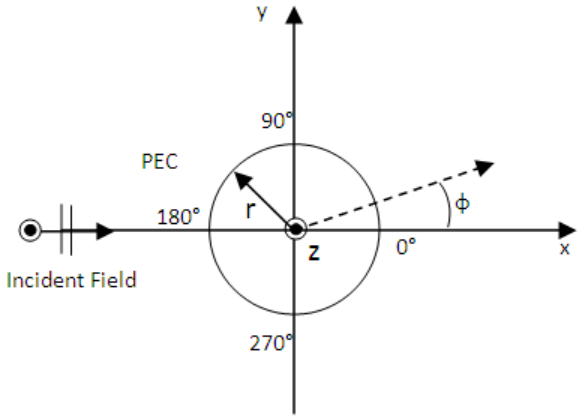

Fig. 1. Plane wave incident on a circular cylinder. The entire cylinder is illuminated.

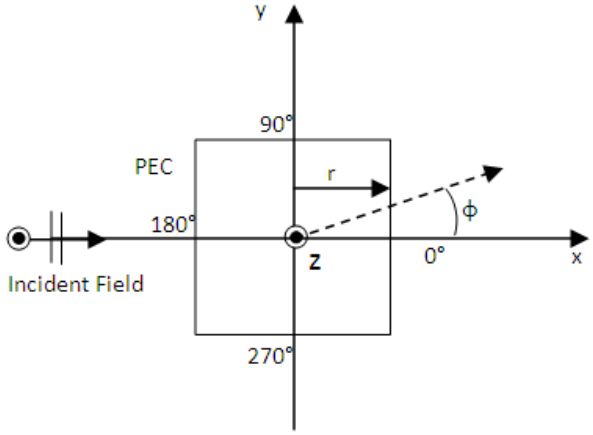

Fig. 2. Plane wave incident on a square cylinder. The entire cylinder is illuminated.

where H_0 is the magnitude of the field and θ_i is the incident angle of the plane wave. By using Ampere's equation, it can be shown that

$$\overrightarrow{E}^i = \frac{1}{j\omega\epsilon}\left[\widehat{a}_\rho \frac{1}{\rho}\frac{\partial H_z^i}{\partial\phi} - \widehat{a}_\phi \frac{\partial H_z^i}{\partial\rho}\right] \quad (3)$$

where E_ρ^i and E_ϕ^i can be derived from this relationship. The sum of the incident and scattered fields must be equivalent to the tangential field, and the scattered magnetic field can be represented by

$$\overrightarrow{H}^s = \widehat{a}_z H_0 \sum_{n=0}^{n=\infty} d_n H_n^{(2)}(\beta\rho) \quad (4)$$

where $H_n^{(2)}$ is the Hankel function and d_n is derived from enforcing the boundary condition for the PEC: the tangential electric field vanishes on the surface of the cylinder. From this boundary condition, the following equation is derived:

$$\overrightarrow{E}^t_\phi(\rho = a) = -\frac{\beta H_0}{j\omega\epsilon}[j^{-n}J_n'(\beta a)e^{jn\phi} + d_n H_n^{(2)'}(\beta a)] = 0 \tag{5}$$

which is satisfied when

$$d_n = -j^{-n}\frac{J_n'(\beta a}{H_n^{(2)'}(\beta a)}e^{jn\phi} \tag{6}$$

so that now, the tangential magnetic field can be derived as

$$H_z^t(\rho = a) = -jH_0\frac{2}{\pi\beta a}\sum_{n=-\infty}^{\infty} j^{-n}\frac{e^{jn\phi}}{H_n^{(2)'}(\beta a)} \tag{7}$$

The surface current on the cylinder is derived as

$$\overrightarrow{J_s} = \widehat{n}\times\overrightarrow{H}^t|_{\rho=a} = \widehat{a}_\phi\frac{j2H_0}{\pi\beta a}\sum_{n=-\infty}^{\infty}\frac{j^{-n}e^{jn\phi}}{H_n^{(2)'}(\beta a)} \tag{8}$$

and the bi-static echo width is represented as

$$\sigma = \lim_{\rho\to\infty}\left[2\pi\rho\frac{|H_z^s|^2}{|H_z^i|^2}\right] \tag{9}$$

$$= \sqrt{\frac{2}{\pi\beta a}}\sum_{n=-\infty}^{\infty} b_n e^{jn\phi} \tag{10}$$

For the TM$_z$ case, the induced surface current and bi-static echo width are similarly derived.

$$\overrightarrow{J}^s = \widehat{a}_z\frac{j2E_0}{\pi\omega\mu a}\sum_{n=-\infty}^{\infty}\frac{j^{-n}e^{jn\phi}}{H_n^{(2)}(\beta a)} \tag{11}$$

$$\sigma = \frac{4}{\beta}\left|\sum_{n=-\infty}^{\infty}\frac{J_n(\beta a)}{H_n^{(2)}(\beta a)}e^{jn\phi}\right|^2 \tag{12}$$

C. MOM Solution

1) TEz MFIE Solution: For a TE$_z$ propagating wave, the magnetic field exists only in the z direction. Using the equivalence principle and boundary conditions for the magnetic field at the conductor surface [3], the magnetic field integral equation can be formulated as

$$H_z^{inc}(t) = -J_t(t) - /left\frac{\partial A_y}{\partial x} - \frac{\partial A_x}{\partial y}/right_{S^+} \tag{13}$$

$$\overrightarrow{A(t)} = \int\widehat{t}(t')J_t(t')\frac{1}{4j}H_0^{(2)}(kR)dt' \tag{14}$$

$$R = \sqrt{[x(t)-x(t')]^2 + [y(t)-y(t')]^2} \tag{15}$$

$$\widehat{t}(t) = \widehat{x}\cos\Omega(t) + \widehat{y}\sin\Omega(t) \tag{16}$$

where t is the position along the surface of the scatterer and $\widehat{t}$ is the unit vector tangent to the surface.

To approximate the surface current J_s, the surface of the PEC shape is segmented into N pieces. Pulse basis functions are used such that within each segment, $p_n(t) = 1$ if t is within cell n, and is 0 otherwise. This gives an expression for the current in terms of a sum of subdomain basis functions:

$$\overrightarrow{J_z}(t) \cong \sum_{n=1}^{N} j_n p_n(t) \tag{17}$$

Using the point matching technique, which is equivalent to using delta testing functions, we can form the method of moments matrix equation as

$$\overline{V} = \overline{\overline{Z}J} \tag{18}$$

with the elements of the matrix equation being

$$V_m = H_z^{inc}(t_m) \tag{19}$$

$$J_n = j_n Z_{mn} = \frac{k}{4j}\int_{celln}(\sin\Omega(t')\frac{x_m - x(t')}{R_m} \tag{20}$$

$$-\cos\Omega(t')\frac{y_m - y(t')}{R_m})H_1^{(2)'}(kR_m)dt'$$

$$Z_{mm} = -1 + \lim_{x\to x_m, y\to y_m}\frac{k}{4j}\int_{cellm}(\sin\Omega(t')\frac{x_m - x(t')}{R_m} \tag{21}$$

$$-\cos\Omega(t')\frac{y_m - y(t')}{R_m})H_1^{(2)'}(kR_m)dt'$$

$$R_m = \sqrt{[x_m(t) - x(t')]^2 + [y_m(t) - y(t')]^2} \tag{22}$$

The limit for the self-term entry can be performed analytically for flat cells so that Z_{mm} is exactly -1/2; this simplification is used in the implementation. This matrix equation is solved for $\overline{J}$, and these values are used to calculate the surface current in (17). Once the current coefficients are known, the bi-static echo width can be approximated by

$$\sigma_{TE}(\phi) \cong \frac{k}{4}\left|\sum_{n=1}^{N} j_n w_n \sin(\Omega_N - \phi)e^{jk(x_n\cos\phi + y_n\sin\phi)}\right|^2 \tag{23}$$

where w_n is the length of segment n.

2) TEz EFIE Solution: Alternatively, an EFIE formulation can be used for the TE$_z$ case. Using the same equivalence principle and boundary conditions for the electric field, the EFIE equation can be written as

$$\widehat{t}\cdot\overrightarrow{E}^{inc} = jk\eta\widehat{t}\cdot\overrightarrow{A} + \widehat{t}\cdot\nabla\Phi_e \tag{24}$$

where the magnetic vector potential and electric scalar potential are, respectively,

$$\overrightarrow{A}(t) = \int\widehat{t}(t')J_t(t')\frac{1}{4j}H_0^{(2)}(kR)dt' \tag{25}$$

$$\Phi_e(t) = \int\frac{\rho_e(t')}{\varepsilon_0}\frac{1}{4j}H_0^{(2)}(kR)dt' \tag{26}$$

$$-j\omega\rho_e = \nabla_s\cdot\overrightarrow{J} = \frac{\partial J_t}{\partial t} \tag{27}$$

$$R = \sqrt{[x(t) - x(t')]^2 + [y(t) - y(t')]^2} \tag{28}$$

where J and ρ_e are the surface current and charge density, respectively.

If pulse basis functions are employed, the discontinuous representation of the current leads to fictitious line charges

between each cell. Therefore, a continuous basis function must be used to represent the current. For this problem, triangle basis functions were chosen. The current density can be written in terms of these functions as

$$\overrightarrow{J_t}(t) \cong \sum_{n=1}^{N} j_n t(t; t_{n-1}, t_n, t_{n+1}) \tag{29}$$

The charge density inside the scalar potential can be written as a combination of pulse functions:

$$\rho_e(t) \cong \frac{-\eta\varepsilon_0}{jk} \sum_{n=1}^{N} j_n \left(\frac{1}{t_n - t_{n-1}} p(t; t_{n-1}, t_n) \right. \tag{30}$$

$$\left. -\frac{1}{t_{n+1} - t_n} p(t; t_n, t_n + 1)\right)$$

Using pulse basis functions, defined between $t_{m-1/2}$ and $t_{m+1/2}$, the matrix equation elements are now

$$V_m = \int_{t_{m-1/2}}^{t_{m+1/2}} \widehat{t}(t) \cdot \overrightarrow{E}^{inc}(t) dt \tag{31}$$

$$Z_{mn} = \frac{k\eta}{4} \int_{t_{m-1/2}}^{t_{m+1/2}} \widehat{t}(t) \cdot \int_{t_{n-1}}^{t_{n+1}} \widehat{t}(t') t(t') H_0^{(2)}(kR_2) dt' dt \tag{32}$$

$$+\frac{\eta}{4k} \frac{1}{t_n - t_{n-1}} \left(\int_{t_{n-1}}^{t_n} H_0^{(2)}(kR_2) dt' - \int_{t_{n-1}}^{t_n} H_0^{(2)}(kR_1) dt' \right)$$

$$-\frac{\eta}{4k} \frac{1}{t_{n+1} - t_n} \left(\int_{t_n}^{t_{n+1}} H_0^{(2)}(kR_2) dt' - \int_{t_n}^{t_{n+1}} H_0^{(2)}(kR_1) dt' \right)$$

The double integral in (32) is computationally expensive, so an approximation is used for the testing process. One approximation is given by [4]:

$$\int_{t_{m-1/2}}^{t_{m+1/2}} \widehat{t}(t) \cdot \int_{t_{n-1}}^{t_{n+1}} \widehat{t}(t') t(t') H_0^{(2)}(kR_2) dt' dt \cong \tag{33}$$

$$[(t_m - t_{m-1/2})\widehat{t}(t_{m-1/2}) + (t_{m+1/2} - t_m)\widehat{t}(t_{m+1/2})]$$

$$\left(\widehat{t}(t_{n-1/2}) \int_{t_{n-1/2}}^{t_n} H_0^{(2)}(k\widetilde{R}) dt' + \widehat{t}(t_{n+1/2}) \int_{t_{n-1/2}}^{t_n} H_0^2(k\widetilde{R}) dt' \right)$$

$$\widetilde{R} = \sqrt{[x(t_m) - x(t')]^2 + [y(t_m) - y(t')]^2} \tag{34}$$

This approximation reduces the double integral to a single integral, making it computationally comparable to the TE MFIE case.

Since the current is now represented in terms of triangular basis functions, the radar cross section is written in terms of an integral as

$$\sigma_{TE}(\phi) \cong \frac{k}{4} \Big| \sum_{n=1}^{N} \int_{t_{n-1}}^{t_{n+1}} [\widehat{y} \cdot \widehat{t}(t') \cos\phi - \widehat{x} \cdot \widehat{t}(t') \sin\phi] j_n \tag{35}$$

$$\times t(t'; t_{n-1}, t_n, t_{n+1}) e^{jk[x(t')\cos\phi + y(t')\sin\phi dt']} \Big|^2$$

3) TMz EFIE Solution: For the TM$_z$ case, it is known that $\nabla \cdot \overrightarrow{J} = 0$, so that the general EFIE can be written as [4]

$$\overrightarrow{E_z}^{inc}(t) = e^{-jk(x\cos\phi^{inc} + y\sin\phi^{inc})} = jk\eta A_z(t) \tag{36}$$

where

$$A_z(t) = \int J_z(t') \frac{1}{4j} H_0^{(2)}(kR) dt' \tag{37}$$

$$R = \sqrt{[x(t) - x(t')]^2 + [y(t) - y(t')]^2} \tag{38}$$

The pulse basis function as defined in the previous sections is implemented so that $J_z(t)$ is defined as with the TE MFIE case. Substituting this into the expression for the incident electric field,

$$\overrightarrow{E_z}^{inc}(t) = jk\eta \sum_{n=1}^{N} j_n \int_{celln} \frac{1}{4j} H_0^{(2)}(kR) dt' \tag{39}$$

The moment method impedance matrix equation elements are now

$$V_m = E_z^{inc}(t_m) \tag{40}$$

$$J_n = j_n \tag{41}$$

$$Z_{mn} = \frac{k\eta}{4} \int_{celln} H_0^{(2)}(kR_m) dt' \tag{42}$$

$$R_m = \sqrt{[x_m(t) - x(t')]^2 + [y_m(t) - y(t')]^2} \tag{43}$$

where x_m and y_m are the center of the segment m. The bistatic echo width can be calculated using

$$\sigma_{TM}(\phi) \cong \frac{k\eta^2}{4} \left| \sum_{n=1}^{N} j_n w_n e^{jk(x_n \cos\phi + y_n \sin\phi)} \right|^2 \tag{44}$$

III. Results

A. Validation

The surface current and bi-static echo width for a circular cylinder with radius 2λ are plotted for both the TE and TM cases using a frequency equal to the speed of light (approximately 30 MHz) and 1001 nodes. The results are shown in Figures 3-6. These plots qualitatively show that the MOM algorithms give accurate, physically sensible results.

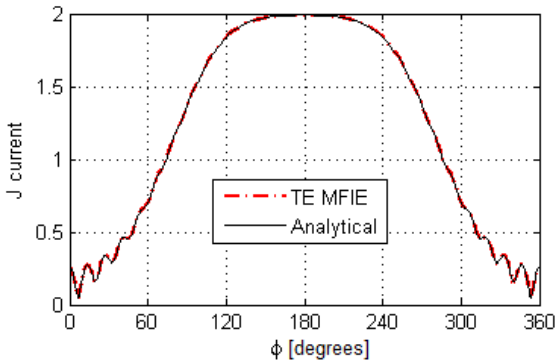

Fig. 3. Surface current of a circular cylinder with r = 2λ, for the TE case.

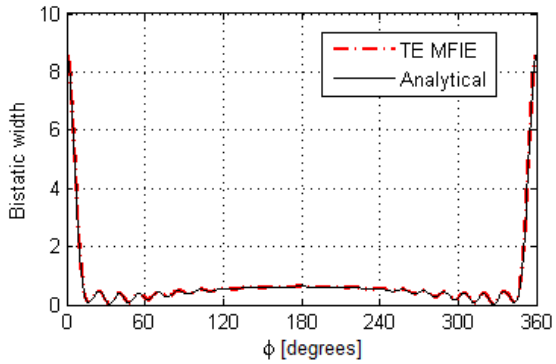

Fig. 4. Bi-static echo width of a circular cylinder with r = 2λ, for the TE case.

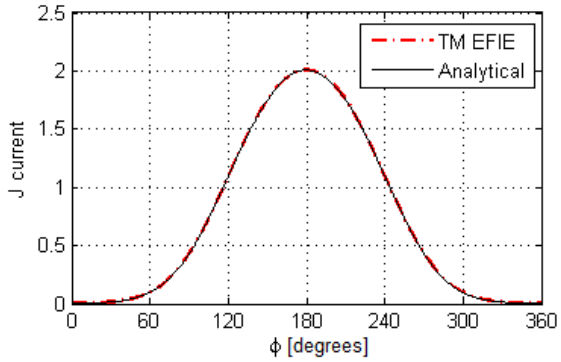

Fig. 5. Surface current of a circular cylinder with r = 2λ, for the TM case.

B. Convergence Analysis

1) Error vs. Nodes: The accuracy of each of the three MOM algorithms described above is evaluated for a circular cylinder of radius 2λ, with the frequency of the incident wave being 1 GHz. The number of nodes is increased and the relative error is calculated by comparing the surface currents and bi-static echo width with the following equation:

$$Error = \frac{||I_{MOM} - R_{analytical}||_2}{||I_{analytical}||_2} \tag{45}$$

The results are shown in Figures 7 and 8. It is evident that the TE EFIE is consistently less accurate than the TE MFIE case; this is expected, since an approximation was used for the double integral in the MFIE formulation. However, without this approximation, the computational complexity order increases by a factor of N. The TM EFIE and TE MFIE algorithms exhibit comparable error.

2) Error vs. Frequency: Because the MOM algorithm is sensitive to the frequency used, the current was simulated by varying the frequency while keeping the radius of the cylinder to be 2 m. The number of nodes was chosen to be 1001.

An additional was experiment was performed, so that the radius of the cylinder was 2λ, varying with frequency.

3) Error vs. Radius: The relative error between the MOM algorithms and the analytical solution was calculated while the radius of the cylinder was varied. The frequency was held constant at 1 GHz, with 1001 nodes used, as the radius

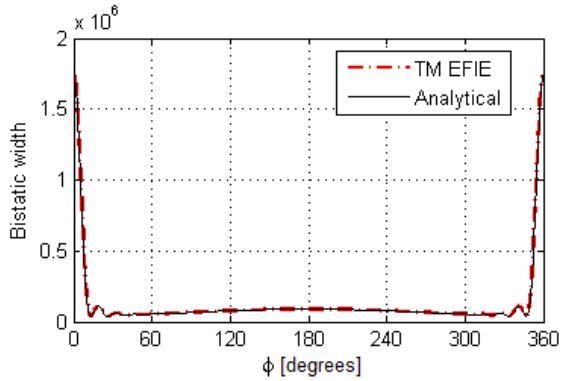

Fig. 6. Bi-static echo width of a circular cylinder with r = 2λ, for the TM case.

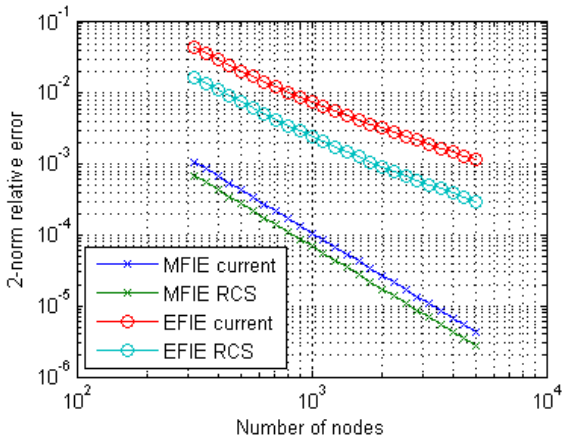

Fig. 7. Relative error for the MOM TE solutions compared to the analytical solutions, vs. number of nodes used in the cylinder discretization.

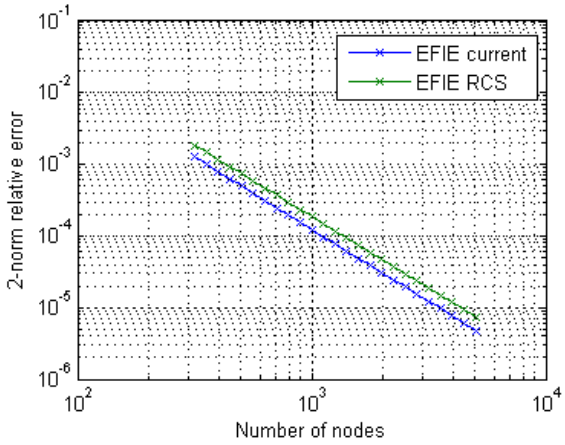

Fig. 8. Relative error for the MOM TM solutions compared to the analytical solutions, vs. number of nodes used in the cylinder discretization.

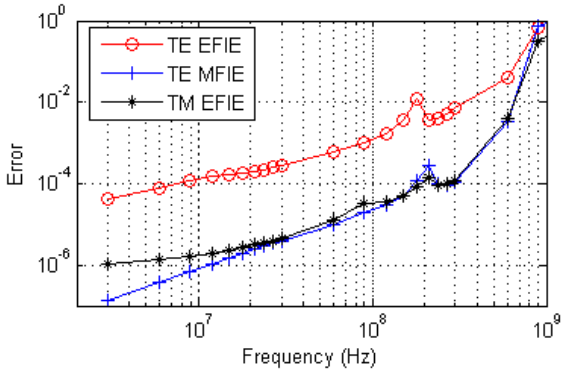

Fig. 9. Relative error for the MOM solutions compared to the analytical solutions for a static radius, vs. frequency of the incident plane wave.

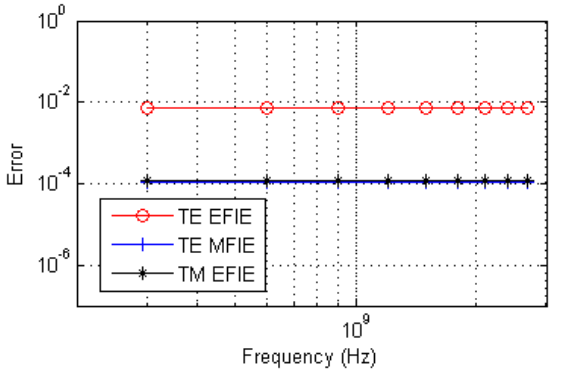

Fig. 10. Relative error for the MOM solutions compared to the analytical solutions for a radius proportional to frequency, vs. frequency of the incident plane wave.

was increased from 0.2λ to 20λ. The results are shown in

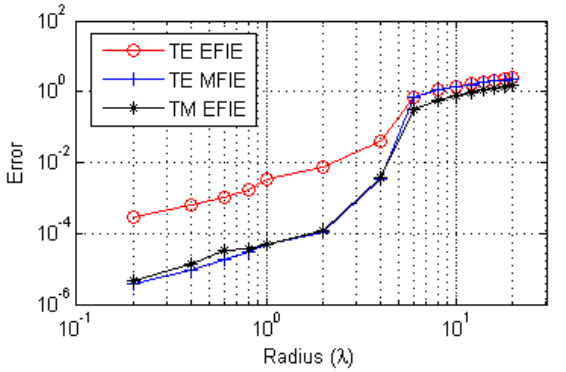

Fig. 11. Relative error for the MOM solutions compared to the analytical solutions, vs. radius of the circular cylinder.

Figure 11. With the same radius, TE MFIE and TM EFIE give essentially the same accuracy, with both performing better than the TE EFIE algorithm. Generally, as the radius becomes larger, the accuracy of all the algorithms is less accurate. This is because the length of each element is increasing while the wavelength is unchanged. For radii of larger than 4λ, the error is too large to provide credible results.

C. Square results

Though an analytical solution does not exist for the scattering from a square cylinder, several papers have examined this phenomena [5–10]. In order to verify the MOM code presented here for both the TE and TM cases, the data from these papers are extracted using data extraction software and plotted against the MOM results.

1) TEz MFIE: The TE_z MFIE code was verified by comparing to results published for a cylinder with half-width $r = \lambda/(2\pi)$ [10]. In this paper, the surface current for half of the illuminated cylinder are calculated. A comparison between these reference results and MOM results is shown in Figure 12. The results from this MOM algorithm line up very well with the reference results.

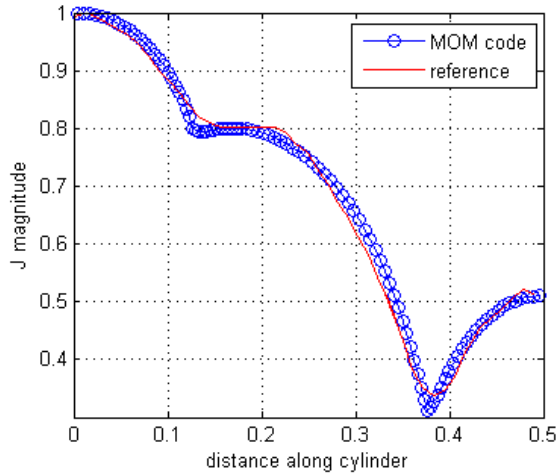

Fig. 12. Surface current on square cylinder, from TEz incident wave. There were 193 nodes in the MOM code used, compared to an integral equation reference solution.

2) TMz EFIE: The TM_z EFIE code was verified by comparing to results published for a cylinder with half-width $r = \lambda/(2\pi)$ [6]. This paper includes simulation results for both the surface current density and the square root of the RCS. These results are shown in Figures 13 and 14; again, the MOM results appear to align very well with the published results.

D. Computational Complexity

For the circular cylinder, the mesh is chosen to be uniform (each segment equal in length); in conjunction with the symmetry of the geometry, the resulting Z-matrix is a complex symmetric Toeplitz matrix. This artifact is very convenient, as only the first row or first column of $\overline{Z}$ needs to be computed and stored. For an n-point quadrature rule, each matrix element takes O(n) operations and Hankel function evaluations for the TE MFIE and TM EFIE methods; for the TE EFIE method, 6 integrals need to be computed for each matrix element, which leads to a considerably larger computation time of O(6n). For an m x m matrix, this leads to O(mn) operations in the matrix fill section of the code. The symmetry in the matrix is suitable for the Conjugate Gradient (CG) method. Because

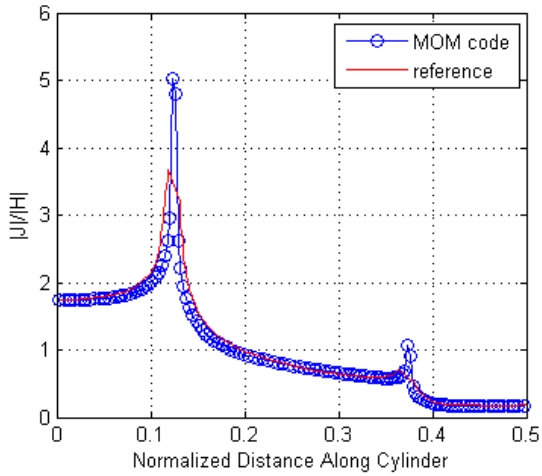

Fig. 13. Surface current on square cylinder, from TMz incident wave. There were 233 nodes in the MOM code used, compared to an FDTD reference solution.

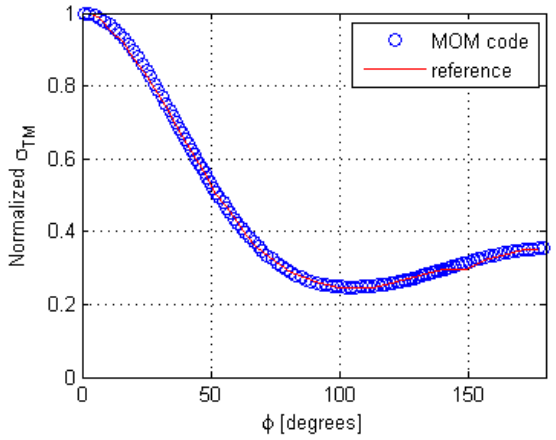

Fig. 14. RCS of square cylinder, from TMz incident wave. There were 233 nodes in the MOM code used, compared to an FDTD reference solution.

of the Toeplitz structure of $\overline{Z}$, the matrix-vector multiplication in the CG method can be simplified by fast Fourier Transform methods; instead of O(m^2) operations, the multiplication can be done in O($m\log(m)$) operations. Thus, for small n, the total complexity for circular cylinders is O($m\log(m)$) operations, with a memory storage requirement of O(m).

For the square cylinder, the mesh is also chosen to be uniform, but the resulting matrix does not have the same Toeplitz structure. Since the the structure is still symmetric, approximately half the elements in the matrix need to be computed, leading to O($nm^2/2$) operations in the matrix fill section. Because the matrix does not have a Toeplitz structure, FFT methods can not be used to decrease the matrix-vector product calculation time. For this geometry, the quasi-minimal residual (QMR) method was used with incomplete LU decomposition for preconditioning; for most matrices, the iteration converged in less than 4 operations. The complexity of QMR in this case is of O(km^2), where k is the number of iterations. For small k and n, this leads to a total complexity of O(m^2) operations. The matrix solver time for each method was calculated with a varying number of nodes. The results are shown in Figure 15 for the circular cylinder and Figure 16 for the square cylinder. These plots both show that

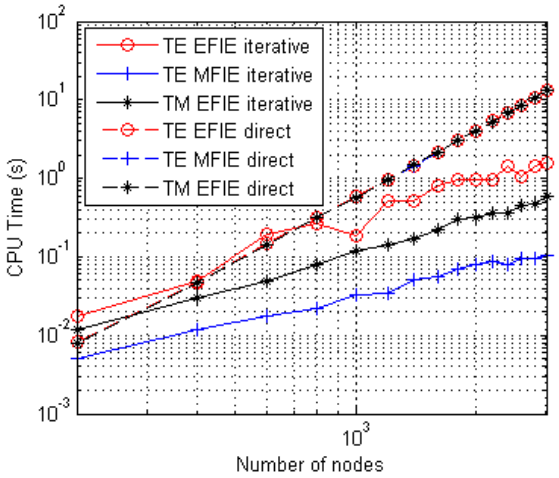

Fig. 15. Solver time vs. number of nodes for a circular cylinder with radius 2λ.

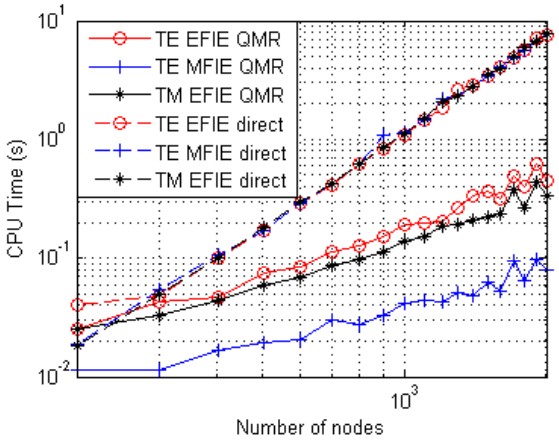

Fig. 16. Solver time vs. number of nodes for a square cylinder with half-width 2λ.

E. Comments on sources of error

For the TE_z EFIE method, triangle basis functions and pulse testing functions are used to discretize the current and form the Z-matrix. Since these functions are of higher order than the pulse basis/delta testing functions used in the TE_z MFIE and TM_z MFIE methods, one would think that the TE_z EFIE formulation would produce more accurate results. However, since the double integral in (32) is approximated, the accuracy of the resulting Z-matrix is compromised. Physically, one can observe that the resulting current contains unwanted oscillations when the curve should be smooth; as the number of nodes increases, the approximation becomes better and the oscillations reduce in intensity.

Although the TE_z MFIE and TM_z EFIE exhibit good

convergence for the 2λ radius test cylinder, it is imperative to note that for certain ratios between frequency and radius, both the EFIE and MFIE formulations alone cannot handle the scattering from the closed PEC structure. For these integral equations, the eigenvalues of the integral operators are

$$\lambda_n^{EFIE,TM} = \frac{1}{2}(\eta\pi ka)J_n(kr)H_n^{(2)}(kr) \quad (46)$$

$$\lambda_n^{MFIE,TE} = \frac{1}{2}(j\pi ka)J_n(kr)H_n^{(2)'}(kr) \quad (47)$$

where J_n and H_n are the nth order Bessel and Hankel functions, respectively. It is obvious that the nth eigenvalue disappears whenever kr is a zero of the nth order Bessel function. This results in a non-unique solution, as any multiple of the eigenfunction corresponding to that eigenvalue can be added to the solution and still satisfy the equation. Internal fields can also be considered solutions to the surface integral equation; the addition of these fields results in the internal resonance phenomenon. This can be observed in the frequency sweep plots, as the relative error stays constant over the graph except at the resonant frequencies.

IV. Conclusion

Three basic MOM algorithms are presented here: both the EFIE and MFIE formulations for the TE_z polarization, and the EFIE formulation for TM_z propagation. These are verified by comparing with an analytical solution (for the circular cylinder) or a reference publication (for the square cylinder). Several experiments were performed with the circular cylinder algorithms to explore the accuracy for different problems, as well as the computational complexity of the methods with and without iterative solvers.

The numerical experiments show that there is a limit to the accuracy of the solvers, as the size of the object becomes too large, or the wavelength becomes too small. Also, the internal resonance phenomena was demonstrated.

References

[1] S. Rao, D. Wilton, and A. Glisson, "Electromagnetic scattering by surfaces of arbitrary shape," *IEEE Transactions on Antennas and Propagation*, vol. 30, no. 3, pp. 409–418, 1982.

[2] A. Glisson and D. Wilton, "Simple and efficient numerical methods for problems of electromagnetic radiation and scattering from surfaces," *IEEE Transactions on Antennas and Propagation*, vol. 28, no. 5, pp. 593–603, Sep 1980.

[3] C. A. Balanis, *Advanced Engineering Electromagnetics*, 1st ed. John Wiley, 1989.

[4] R. M. Andrew F. Peterson, Scott L. Ray, *Computational Methods for Electromagnetics*. Universities Press, 2001.

[5] N. Lucanu, H. Baudrand, D. Cepareanu, and P. Gasner, "Scattering by a 2D square section metallic obstacle," in *International Symposium on Signals, Circuits and Systems*, vol. 2, 2003.

[6] K. Umashankar and A. Taflove, "A Novel Method to Analyze Electromagnetic Scattering of Complex Objects," *IEEE Transactions on Electromagnetic Compatibility*, vol. 24, no. 4, pp. 397–405, Nov. 1982.

[7] V. Shankar, W. Hall, and A. Mohammadian, "A time-domain differential solver for electromagnetic scattering problems," *Proceedings of the IEEE*, vol. 77, no. 5, pp. 709–721, May 1989.

[8] M. Hirose, M. Miyake, J. Takada, and I. Arai, "On applicability of the integral equation formulation of the measured equation of invariance to 2D scattering objects," *IEICE Transactions on Communications*, vol. 82, pp. 645–654, 1999.

[9] M. Lucido, G. Panariello, and F. Schettino, "Analysis of the electromagnetic scattering by perfectly conducting convex polygonal cylinders," *IEEE Transactions on Antennas and Propagation*, vol. 54, no. 4, pp. 1223–1231, April 2006.

[10] K. Mei and J. Van Bladel, "Scattering by perfectly-conducting rectangular cylinders," *IEEE Transactions on Antennas and Propagation*, vol. 11, no. 2, pp. 185–192, Mar 1963.